Effect of Wall Temperature on Hypersonic Gas Flow Past a Compression Ramp Using Quasi-Gas Dynamic Equations

Nhu T. Q. Tran[1] and Nam T. P. Le[1*]
[1]Faculty of Aeronautical Engineering, Vietnam Aviation Academy, Viet Nam
[*]Corresponding Author / E-mails: nhuttq@vaa.edu.vn, namltp@vaa.edu.vn

Manuscript received: July, 2022 / Revised: October 01, 2022 / Accepted: November 15, 2022

ABSTRACT

Numerical simulations of hypersonic rarefied gas flows are important for the aerodynamic design of re-entry vehicles. An investigation numerically of the effect of the wall temperature on the separation flow and the surface quantities of hypersonic gas flow past a large angle compression ramp. The numerical solutions are carried out using the Quasi-Gas Dynamic (QGD) model, which includes the nonequilibrium boundary conditions. Three wall temperatures of 300K, 500K, and 800K are adopted to conduct the numerical investigations. The gas flow is Mach number 6, and nitrogen is the working fluid. The slip velocity and surface gas temperature of the QGD and DSMC solutions give a good agreement. The simulation results show the wall temperature is less sensitive to the slip velocities and significantly affects the surface pressures and gas temperatures. Increasing the wall temperature decreases the recirculation zone size due to the ramp's large angle.

KEYWORDS: Quasi-Gas Dynamic (QGD) model, compression ramp, wall temperature, recirculation zone length, surface quantities

NOMENCLATURE

c_v = Specific heat of the gas at the constant volume
e = Internal energy
k = Thermal conductivity
Pr = Prandtl number
R = Specific gas constant
Sc = Schmidt number
u = Velocity
ρ = Density
δ = Adiabatic exponent
γ = Specific heat ratio
α = Small positive constant
Δ_h = Computational space step

1. Introduction

Hypersonic gas flow simulations are essential for the aerodynamic design of re-entry vehicles. Hypersonic (rarefied) gas flows are classified into four different regimes, and the Knudsen number, Kn, expresses these regimes. It is calculated by the ratio of gas mean free path to a characteristic body length. The number, Kn, indicates the different regimes as 1) $0.0001 \leq Kn \leq 0.01$ (continuum), $0.01 \leq Kn \leq 0.1$ (slip), $0.1 \leq Kn \leq 10$ (transitional), and $Kn \geq 10$ (free molecules). Theoretically, two approaches to solving the rarefied gas flows are the Direct Simulation Monte-Carlo (DSMC) (Bird, 1990) and Computational Fluid Dynamics (CFD). The DSMC approach has been successfully solved for the four gas flow regimes, especially the high-speed viscous gas flows (Pham et al., 1989; Zhang et al., 2019; Wu et al., 2003). The DSMC approach successfully produced the space shuttle flight data to match the experimental data. It also perfectly predicted the molecular velocity distribution function method in the shock wave structure compared to the experiment (Pham et al., 1989). Its computational effort is quite higher than the CFD continuum approach, however. It has been proven that the DSMC approach produces the computational results in simulations of the hypersonic (rarefied) gas flows more precisely than the CFD approach (Zhang et al., 2019; Wu et al., 2003). So, the DSMC data have been chosen as a benchmark to validate the CFD data. The CFD approach (e.g., Navier-Stokes (NS) model) with nonequilibrium boundary conditions may successfully capture the hypersonic gas flows up to the slip regime. The Quasi-Gas Dynamic (QGD) model is also developed from the fluid continuum theory and is different from the Navier-Stokes model by additional dissipative terms (Elizarova et al., 1995; Kraposhin et al., 2018). The QGD model was recently implemented and solved numerically in open-source OpenFOAM software (OpenFOAM, 2022), named the QGDFoam solver (Kraposhin et al., 2018) for simulating the compressible gas flows as an alternative CFD approach.

Appropriately selecting the nonequilibrium boundary conditions is critical to obtaining good computational results in the CFD approach for hypersonic gas flows. The conditions consist of the slip and jump boundary conditions for the velocity and temperature, respectively. The literature also proved that the no-slip/jump simulations could not use for simulating hypersonic viscous gas flows (Le et al., 2012). The CFD simulation results in high-speed gas flows show that the viscous heat generation (shear work) must be included in the temperature jump boundary condition (Le et al., 2017). Therefore, the first-order nonequilibrium boundary conditions used in the present work are the Maxwell slip condition (Maxwell, 1879) and a modified Smoluchowski jump condition (Le et al., 2017), including the viscous heat generation. The QGD model included the nonequilibrium boundary conditions that will be used to simulate the hypersonic (rarefied) gas flows past a compression ramp to enhance the application of this QGD model. The challenge of the numerical simulations of the gas flows past a compression ramp is the precise prediction of the recirculation zone. Moreover, there is also a shock-shock interaction in this case. Research has mostly investigated the recirculation zone due to a small angle of the compression ramp (≤ 30o.) under supersonic gas flows. Meanwhile, a few researchers have conducted hypersonic gas flows past a large-angle compression ramp (≥ 30o.) (Lu et al., 2022). The configuration of the compression ramp in (Lo et al., 2014) with a large angle of 35o is adopted in the current study. The external wall temperature, Tw, of hypersonic vehicles will vary different values in the flight due to various regimes of the gas flows in the atmosphere. In the current work, the effect of the wall temperature on the recirculation zone size, the shock wave structure, and the surface quantities such as the slip velocity, surface gas temperature, and pressure will be numerically investigated. The surface pressure is used to compute the aerodynamic forces, and a maximum surface gas temperature is essential to designing thermal protection systems for hypersonic vehicles. Three wall temperatures, Tw = 300K, 500K, and 800K, are selected to simulate the nitrogen gas flow at a Mach number of 6 for this investigation. The QGD model simulation results with the nonequilibrium boundary conditions are validated with the DSMC data.

2. Quasi-Gas Dynamic (QGD) model

The equations of the QGD model are presented in the conservation laws as follows (Kraposhin et al., 2018),

Mass conservation

$$\frac{\partial \rho}{\partial t}+\nabla\cdot\mathbf{j}_m=0, \tag{1}$$

where the symbol '·' denotes the inner product, and mass flux density jm is computed by (Kraposhin et al., 2018),

$$\mathbf{j}_m=\rho\mathbf{u}-\varepsilon\left(\nabla\cdot\left(\rho\mathbf{u}\mathbf{u}\right)+\nabla p\right), \tag{2}$$

and the additional dissipative coefficient, ε, is calculated (Kraposhin et al., 2018),

$$\varepsilon=\frac{\mu}{pSc}+\alpha\frac{\Delta h}{\sqrt{\gamma RT}}, \tag{3}$$

Momentum conservation (Kraposhin et al., 2018)

$$\frac{\partial\rho\mathbf{u}}{\partial t}+\nabla\cdot\left(\mathbf{j}_m\mathbf{u}\right)+\nabla p=\nabla\cdot\mathbf{\Pi}_{NS}+\nabla\cdot\mathbf{\Pi}_{QGD}, \tag{4}$$

where the NS stress tensor, ΠNS, is presented by

$$\mathbf{\Pi}_{NSF}=\mu\left(\nabla\mathbf{u}+\left(\nabla\mathbf{u}\right)^T-\mathbf{I}\frac{2}{3}\nabla\cdot\mathbf{u}\right), \tag{5}$$

where the transpose is denoted by the superscript T. The QGD stress tensor, ΠQGD, is determined by (Kraposhin et al., 2018),

$$\mathbf{\Pi}_{QGD}=\varepsilon\mathbf{u}\rho\left(\mathbf{u}\cdot\nabla\mathbf{u}+\frac{1}{\rho}\nabla p\right)+\varepsilon\mathbf{I}\left(\mathbf{u}\cdot\nabla p+\delta p\nabla\cdot\mathbf{u}\right). \tag{6}$$

Energy conservation (Kraposhin et al., 2018),

$$\begin{aligned}\frac{\partial\rho E}{\partial t}+\nabla\cdot\left(\mathbf{j}_m E+\mathbf{u}p\right)+\nabla\cdot\mathbf{q}_{NS}+\nabla\cdot\mathbf{q}_{QGD}\\ =\nabla\cdot\left(\mathbf{\Pi}_{NS}\cdot\mathbf{u}\right)+\nabla\cdot\left(\mathbf{\Pi}_{QGD}\cdot\mathbf{u}\right),\end{aligned} \tag{7}$$

where total energy E = e + 0.5ρ|u2|, and the heat flux NS, qNS, is expressed by

$$\mathbf{q}_{NS}=-k\nabla T, \tag{8}$$

and the heat flux QGD, qQGD, is computed as

$$\mathbf{q}_{QGD}=-\varepsilon\mathbf{u}\rho\left(\mathbf{u}\cdot\nabla e-p\mathbf{u}\cdot\nabla\left(\frac{1}{\rho}\right)\right). \tag{9}$$

It is noted that the QGD model will become the NS model when the coefficient, ε, is equal to zero. The non-negative dissipative functions such as jm, qQGD, and ΠQGD are non-negative to ensure the dissipative term existence for the QGD model (Kraposhin et al., 2018). The pressure, p, is computed by the inviscid model as follows,

$$p=\rho RT, \tag{10}$$

The viscosity is described as a temperature function, $\mu\to\mu+Sc^{QGD}p\varepsilon$, where ScQGD is a positive tuning coefficient (Kraposhin et al., 2018), and the Sutherland law computes μ. The QGD model was numerically embedded in OpenFOAM using the finite volume method, namely the QGDFoam solver (Kraposhin et al., 2018).

3. Nonequilibrium boundary conditions

This section presents the nonequilibrium boundary conditions (BCs). The Maxwell slip condition is generally represented as (Maxwell, 1879),

$$\begin{aligned}\mathbf{u}+\left(\frac{2-\sigma_u}{\sigma_u}\right)\lambda\nabla_{\mathbf{n}}\left(\mathbf{S}\cdot\mathbf{u}\right)\\ =\mathbf{u}_w-\left(\frac{2-\sigma_u}{\sigma_u}\right)\lambda\left(\mathbf{S}\cdot\left(\mathbf{n}\cdot\mathbf{\Pi}_{mc}\right)\right)-\frac{3}{4}\frac{\mu}{\rho}\frac{\mathbf{S}\cdot\nabla T}{T}.\end{aligned} \tag{11}$$

The right-hand side of equation (11) consists of three terms (in order): the wall velocity, uw, curvature effect, and thermal creep. The tensor S = I-nn ensures the tangential velocity on the surface; I is the identity tensor, n (unit normal vector) is positive in the outward direction of the computational domain, and

tensor Πmc is computed by,

$$\boldsymbol{\Pi}_{mc} = \mu\left(\left(\nabla\mathbf{u}\right)^{T} - \mathbf{I}\frac{2}{3}\nabla\cdot\mathbf{u}\right). \quad (12)$$

The tangential momentum accommodation coefficient, σu, denotes the proportion of molecules reflected from the surface diffusely, then specularly (equal to 1−σu), and $0 \le \sigma u \le 1$. The Maxwellian mean free path, λ, of the gas flow is expressed by (Le et al., 2012),

$$\lambda = \frac{\mu}{\rho}\sqrt{\frac{\pi}{2RT}}. \quad (13)$$

The temperature jump condition has been deployed by considering shear work (viscous heat generation) at the surface as a modified Smoluchowski jump condition (Le et al., 2017). It is better than the Smoluchowski jump condition (von Smoluchwoski, 1898) in predicting the surface gas temperatures for high-speed viscous gas flows and is adopted for the simulations using the QGD model and is shown as follows,

$$T + \left(\frac{2-\sigma_T}{2\sigma_T}\right)\frac{\gamma}{\gamma-1}\frac{\lambda}{\mathrm{Pr}}\nabla_n T = T_w - \left(\frac{2-\sigma_T}{2\sigma_T}\right)\frac{\gamma}{\gamma-1}\frac{\lambda}{\mu c_v}\left(\mathbf{S}\cdot\left(\mathbf{n}\cdot\boldsymbol{\Pi}_{NS}\right)\cdot\mathbf{u}\right), \quad (14)$$

where the second term on the right-hand side indicates the viscous heat generation. Equation (14), which does not include the viscous heat generation term, yields the standard Smoluchowski jump condition. The thermal accommodation coefficient, σT, denotes an energy exchange between the gas molecules and the wall (surface), its value ranging from 0 to 1. The value of unity perfectly indicates the energy exchange, and there is no energy exchange σT = 0.

4. Mesh and numerical setup

The numerical setup for a compression ramp and its geometrical dimensions are shown in Figure 1. The freestream conditions (p, T, u) of gas flow are held at the inlet throughout the calculated process. The nonequilibrium boundary conditions are set to the wall (surface) for (T, u), and a zero normal gradient condition is applied to the remaining boundaries so that they disappear at those boundaries. The latter condition is also applied to all boundaries for the pressure. A structured mesh is designed to wrap around the shock wave. A typically structured mesh of a compression ramp case is presented in Figure 2. Mesh independence is conducted and presented as an illustration with four different meshes. Figure 3 shows the slip velocity distributions of different mesh sizes of the case Tw = 300K with the freestream conditions p = 0.82Pa, T = 57K, u = 924m/s, Kn = 0.01. There is a 5% in difference of the slip velocities between two meshes Δx = Δy = 0.5mm and Δx = Δy = 0.25mm. So, a final mesh selected to achieve a convergent solution is the mesh size Δx = Δy = 0.25mm.

5. Simulation results

Simulation results using the QGD approach and the DSMC solution are presented in this section. The freestream conditions of the nitrogen gas flow, p = 0.82Pa, T = 57K, u = 924m/s (e.g. Mach number of 6), Kn = 0.01 are adopted for the current work. Three different wall temperatures, Tw = 300, 500, and 800K, are chosen to investigate their effect on the separation flow and the surface quantities. The coefficients σu and σT are set to be the same for CFD and DSMC solutions. So, the value of 1 is chosen for them. The nitrogen gas flow at Mach number 6 past a large-angle compression ramp is numerically simulated. The ramp structure has a flat plate and ramp parts. The characteristic body length to calculate the Knudsen number, Kn, is the length of the flat plate part, L1, seen in Figure 1.

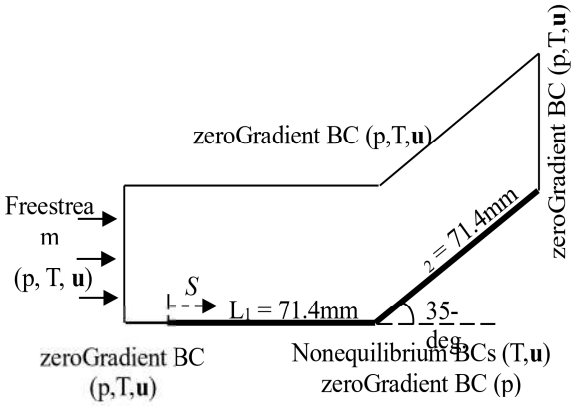

Figure 1. Numerical setup of a compression ramp.

The solver QGDFoam including the nonequilibrium boundary conditions generates the QGD results. The solver dsmcFoam is used to produce the DSMC data in OpenFOAM. The collision model Variable Hard Sphere (VHS) and the final mesh size of a one-third mean free path, λ, are selected for the DSMC simulations. The hypersonic gas flow past a compression ramp is complicated because there is a shock-shock interaction, and appears the separation flow around the corner. The calculated QGD and DSMC results of the surface quantities are plotted against the normalized distance, S/L, where S and L are the running distance and the total length of the ramp, respectively, as seen in Figure 1.

The calculated surface pressures of the DSMC and QGD solutions are presented in Figure 4. The QGD simulations predict higher pressures near the leading edge than DSMC due to the high nonequilibrium effect (Le et al., 2019). Past the leading-edge, all calculated QGD pressures gradually decrease to $S/L \le 0.18$ during the DSMC data increase. Past this location, S/L = 0.18, all QGD and DSMC pressures rapidly increase towards the location, S/L = 0.82. The pressure increase may be due to the separation flow (recirculation zone) and the ramp's existence. The DSMC pressures are higher than those of the QGD model in the range of S/L from 0.3 to 0.9. After that, all of them will decrease due to the imposed boundary conditions at the outlet of the computational domain. In the QGD model, the pressure is calculated by the inviscid model, which is weakly true for viscous gas. So, the QGD simulations overpredict the pressure at the leading edge. While the DSMC pressure is integrated by the collision operators (Le et al., 2019). So the QGD pressures do not agree with those of the DSMC solutions. It is seen that the wall temperature has significantly

impacted the DSMC and QGD surface pressures.

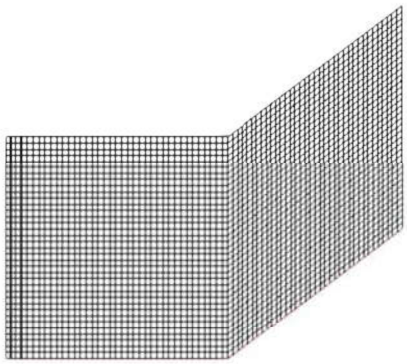

Figure 2. A typically structured mesh of the ramp case (every fifth line presented).

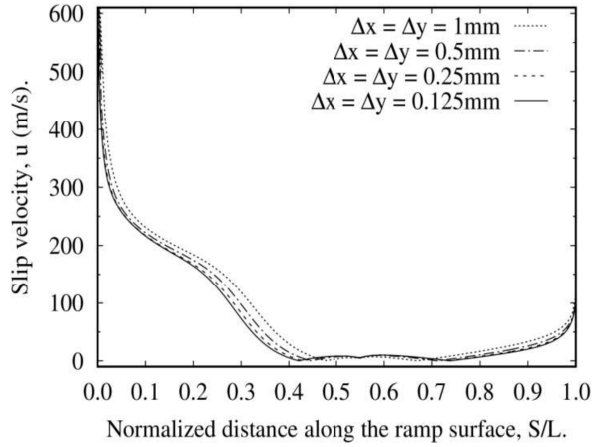

Figure 3. Slip velocities along the surface with different meshes

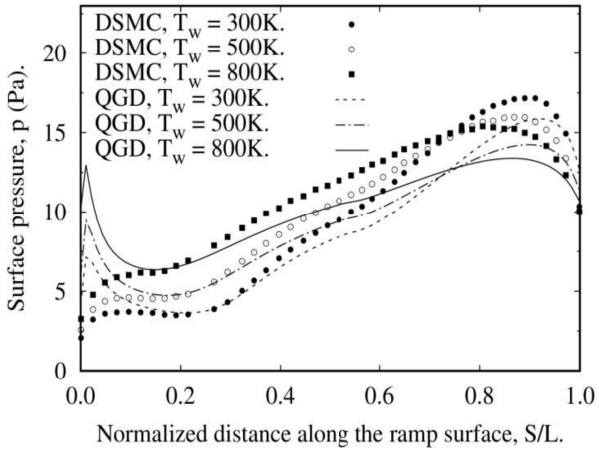

Figure 4. Calculated pressures along the ramp surface

The QGD surface gas temperature will be compared with the DSMC translational temperature. Their distributions are found in Figure 5. As expected, the increase in the wall temperature will increase all QGD and DSMC temperatures because the wall temperature is an input of the jump conditions in both solutions. At the leading edge, the DSMC temperatures are higher than those of QGD simulations. This may be explained by the surface-reflected gas particles, in the DSMC method, colliding with the oncoming freestream gas particles before they detect the presence of the surface at the leading edge. Therefore, the temperatures of the surface-reflected particles near the surface remain high until sufficient interactions occurred with the surface at Tw (Moss et al., 1991; Le et al. 2019). Past the leading edge, they all approach nearly constant finite values past the leading edge towards the location

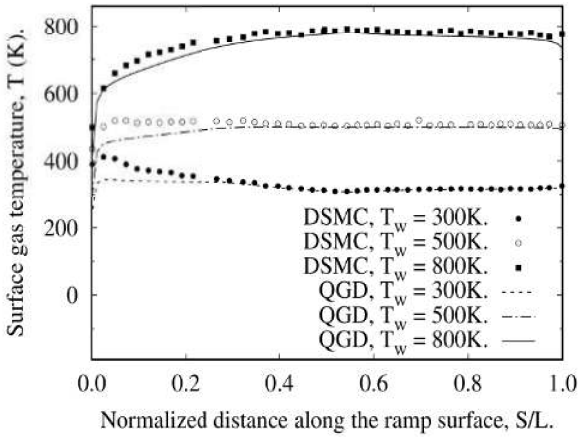

Figure 5. Gas temperatures along the ramp surface.

Figure 6 presents the DSMC and QGD slip velocities. Near the leading edge, the QGD and DSMC slip velocities are highest due to the high viscous effect and rapidly decrease to S/L = 0.4, where the gas flows will enter the recirculation zone. Interestingly, the slip velocities are negative around the corner (S/L = 0.5). This indicates a recirculation zone occurs over the surface and is in the vicinity of the ramp's corner. The separation point locates on the flat plate, and the reattachment point exists on the ramp surface. The zero slip velocities denote the separation and reattachment points. Then, the recirculation zone size is a normalized distance denoted by the presence of the negative velocity. Values of these QGD and DSMC lengths are 1) 0.3 and 0.24, respectively, for the case Tw = 300K, 2) 0.27 and 0.19 for the case, Tw = 500K, and 3) 0.23 and 0.17 for the case, Tw = 800K. Past this zone, the velocities increase towards the location S/L = 1, which is slower than those near the leading edge by the ramp existence. The DSMC and QGD slip velocities agree well along the ramp surface. The DSMC and QGD calculations show that the wall temperature is less sensitive to the slip velocity. The recirculation zone lengths are enlarged in subfigures to see the effect of wall temperature on them. With the hotter wall, the zone length is shorter. The QGD velocity profiles in the recirculation zone have the biquadratic function profile. Because the gas flows in this zone slip down from the ramp surface and collide at the corner. So, the flow kinetic energy is lost due to this sudden impact, decreasing the slip velocity. Then, the gas flows continue to slip over the flat plate surface due to the effect of this zone with a bit velocity increase. Finally, their magnitudes decrease towards the separation point (Le and Huynh, 2022).

For completeness, the translational DSMC and QGD

temperature contours and the velocity streamline overlaid on the contours of three cases Tw = 300K, 500K, and 800K are presented in Figure 7. The DSMC and QGD solutions well capture the shock wave and shock-shock interaction. There are changes in the shock wave structure near the surface due to the effect of the wall temperature. The shock-shock interactions of the DSMC approach are stronger than those of the QGD. Overall, the DSMC solution predicts higher temperatures than the QGD solution in the shock region. The streamlines also show the recirculation zones, and the DSMC ones are smaller than those of the QGD simulations. The recirculation region sizes experience a reduction in the corresponding wall temperature increase. Interestingly in the previous work, the increase in the wall temperature will increase the recirculation zone size for hypersonic gas flow past a small-angle compression ramp (≤ 300) (Exposito et al., 2021). In the present work, the recirculation zone size decreases when the wall temperature increases in the presence of the hypersonic gas low past a large-angle compression ramp, particularly 350. Therefore, the decrease in the zone size may be due to the ram's large angle (≥300).

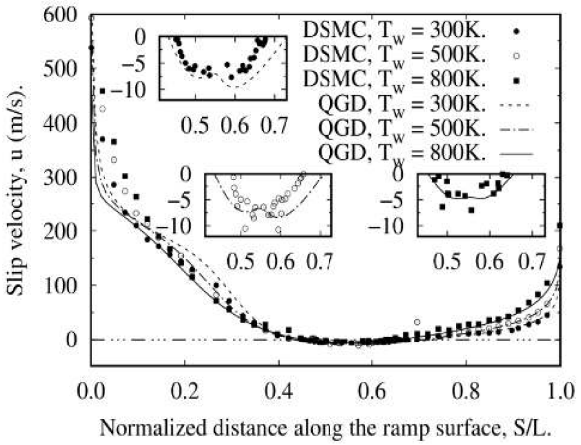

Figure 6. Calculated pressures along the ramp surface.

6. Conclusion

Hypersonic nitrogen gas flow past a large-angle compression ramp has been numerically simulated using both DSMC and QGD approaches. Several wall temperatures are investigated to observe the separation flow. The increase in wall temperature decreases the separation length due to the ramp's large angle and changes the shock wave structure near the surface. Slip and jumpy conditions predict the gas temperature and slip velocity well compared with the DSMC data. The DSMC and QGD surface quantities near the leading edge significantly differ due to the high nonequilibrium effect. The wall temperature significantly impacts the recirculation zone size and the gas pressure and temperature. It does not significantly affect the slip velocity. Finally, using the QGD equations with nonequilibrium boundary conditions as an alternative CFD method for simulating hypersonic gas flows.

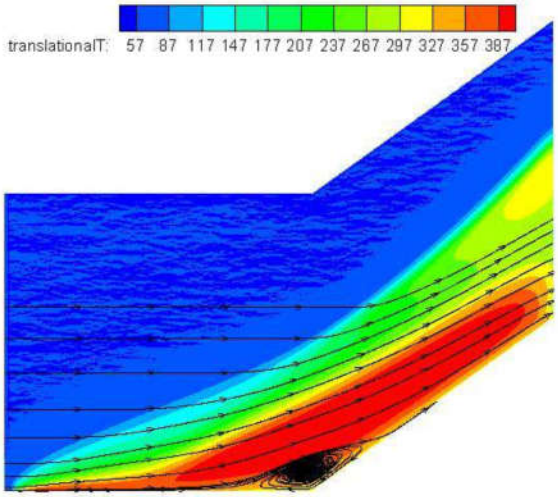

a) DSMC, T_w = 300K.

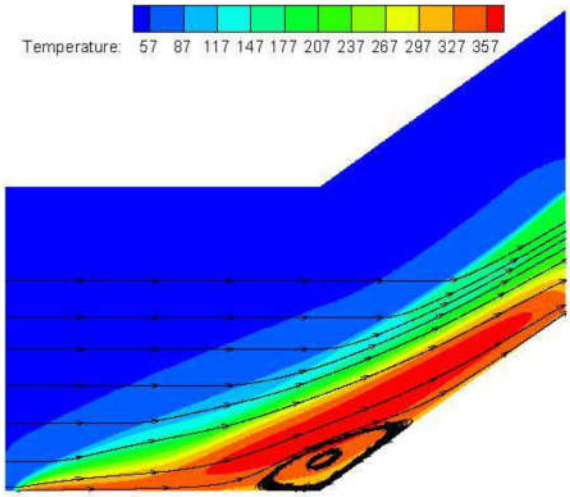

b) QGD, T_w = 300K.

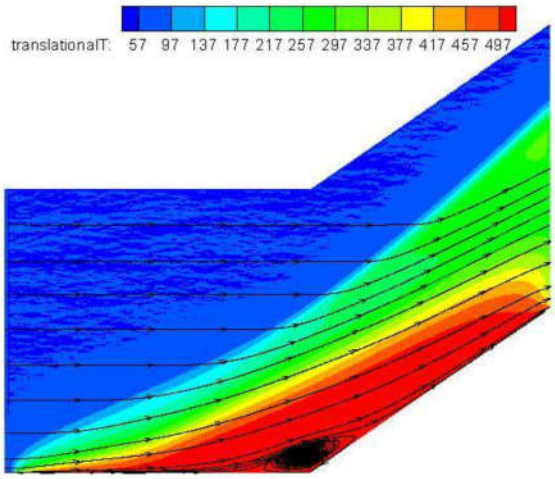

c) DSMC, T_w = 500K.

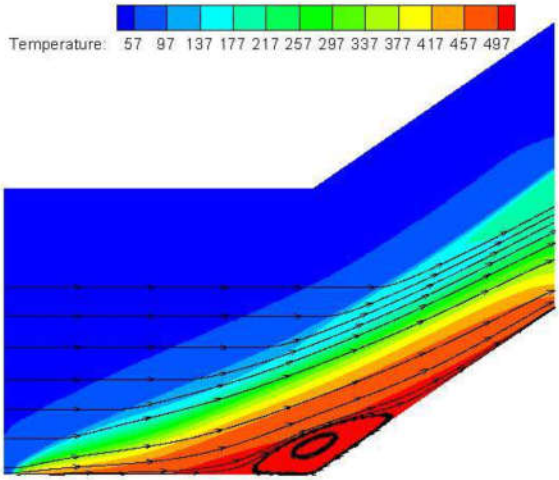

d) QGD, T_w = 500K.

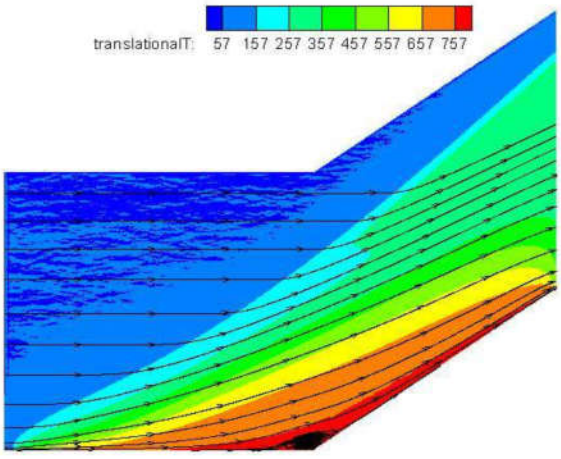

e) DSMC, T_w = 800K.

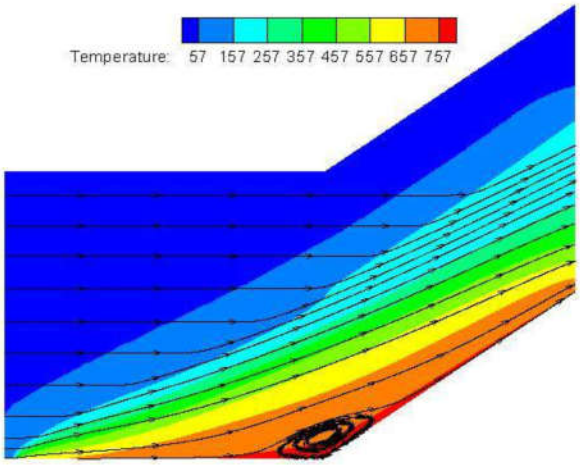

f) QGD, T_w = 800K.

Figure 7. Translational DSMC and QGD temperature contours and velocity streamlines.

References

1. Bird, G. (1990), "Application of the direct simulation Monte Carlo method to the full shuttle geometry", AIAA paper, No. 1990–1692.
2. Pham V. D., Erwin, D., and Muntz, E. P. (1989), "Nonequilibrium molecular motion in a hypersonic shock-wave", Sciences, Vol. 245, pp. 624–626.
3. Zhang, J., John, B., Pfeiffer, M., Fei, F. and Wen, D. (2019), "Particle-based hybrid and multiscale methods for nonequilibrium gas flows", Advances in Aerodynamics, Vol. 1, pp. 1-12.
4. Wu, J. S. and Tseng, K. C. (2003), "Parallel particle simulation of the near-continuum hypersonic flows
5. over compression ramps", Journal of Fluids Engineering, Vol. 125, pp. 181 -188.
6. Elizarova, T. G., Graur, I., Lengrand, J. and Chpoun, A. (1995), "Rarefied gas flow simulation based on quasi gas dynamic equations", AIAA Journal, Vol. 33, pp. 2316–2324.
7. Kraposhin, V. M., Smirnova, E. V., Elizarova, T. G. and Istomina, M. A. (2018), "Development of a new OpenFOAM solver using regularized gas dynamic equations", Computer & Fluids, Vol. 166, pp. 163–175.
8. OpenFOAM, www.openfoam.org (accessed 12 June 2022).
9. Le, N. T. P., Greenshields, C. J. and Reese, J. M. (2012), "Evaluation of nonequilibrium boundary condition in simulating hypersonic gas flows", Progress in Flight Physics, Vol. 3, pp. 217–230.
10. Le, N. T. P., Vu, N. A. and Loc, L. T. (2017), "New type of Smoluchowski temperature jump condition considering the viscous heat generation", AIAA Journal, Vol. 55, pp. 474 – 483.
11. Maxwell, J. C. (1879), "On stresses in rarefied gases arising from inequalities of temperature", *Philosophical Transactions of the Royal Society A,* Vol. 170, pp. 231–256.
12. Lu, J., Yang, H., Zhang, Q., Wen, X. and Yin, Z. (2022), "Experimental investigation of hypersonic laminar flow over a compression ramp", Journal of Fluids Engineering; Vol. 144, 021205-1.
13. Lo, M. C., Sua, C. C., Wu, J. S. and Kuo, F. A. (2014), "Development of parallel direct simulation Monte Carlo method using a cut-cell Cartesian grid on a single graphics processor", Computer & Fluids, Vol. 101, pp. 114 – 125.
14. von Smoluchowski, M. (1898), "Über wärmeleitung in verdünnten gasen", *Annalen der Physik und Chemie*, Vol. 64, pp. 101 – 130.
15. Le, N. T. P., Roohi. E. and Tran, T. N. (2019), " Comprehensive assessment of newly-developed slip-jump boundary conditions in high-speed rarefied gas flow simulations", *Aerospace Sciences and Technology, Vol.* 91, pp. 656–668.
16. Moss, J. N., Price, J. M. and Chun, C. H. (1991), "Hypersonic rarefied flow about a compression corner - DSMC simulation and experiment", AIAA Paper, No. 91-1313.
17. Le N. T. P., and Huynh P. T., (2022), "High-speed rarefied gas flow simulations using Quasi-Gas Dynamic equations with slip and jump boundary conditions", Proceedings of the Institution of Mechanical Engineers, Part G: Journal of Aerospace Engineering. First online, (https://doi.org/10.1177/09544100221103752).
18. Exposito, D., Gai, S. L. and Neely, A. J. (2021), "Wall temperature and bluntness effects on hypersonic laminar separation at a compression corner", Journal of Fluid Mechanics, Vol. 922, pp. A1.1-37.